03,09,12

# Features of the Energy Band Structure of the InAsSbP Epilayer Deposited on a Surface of the $InAs_{1-y}Sb_y$ Solid Solution

© V.V. Romanov, K.D. Moiseev ¶

Ioffe Institute,
St. Petersburg, Russia

¶ E-mail: mkd@iropt2.ioffe.ru

Received June 13, 2023
Revised August 14, 2023
Accepted September 13, 2023

The photoluminescence spectra of narrow-gap InAs/InAsSbP/$InAs_{0.95}Sb_{0.05}$/InAsSbP heterostructures obtained by vapor-phase epitaxy from organometallic compounds on an InAs substrate were studied in a wide temperature range $T = 4-300$ K. The influence of the composition and structure of the matrix surface enriched with antimonide-arsenides on the composition and luminescent properties of the $InAs_{1-x-y}Sb_yP_x$ epitaxial layer during its deposition by the MOVPE method was revealed. The ratio between the concentrations in the solid phase of narrow-gap and wide-gap compounds that form a quaternary solid solution affects the effective energy of location for charge carrier localization centers in the band gap of a quaternary solid solution.

**Keywords:** photoluminescence, antimonides, arsenides, radiative transitions.

DOI: 10.61011/PSS.2023.10.57214.116

## 1. Introduction

The $InAs_{1-x-y}Sb_yP_x$ quaternary solid solutions are one of the basic elements of narrow-gap epitaxial heterostructures based on indium arsenide compounds for the creation of optoelectronic devices operating in the mid-infrared (IR) range $2-6\,\mu$m. Most often they are used as potential energy barriers to ensure localization of charge carriers in the narrow-gap active region of light-emitting diodes (LEDs), lasers and photodiodes [1–6]. Epitaxial layers in the system of In-As-Sb-P solid solutions isomorphic to the InAs substrate can be obtained by metal-organic vapor-phase epitaxy (MOVPE) in a wide range of compositions ($0 < x < 0.72$) [7,8]. At the same time, during the growth process the effect of self-organization of the solid phase of the $InAs_{1-x-y}Sb_yP_x$ epitaxial layer was discovered, which was due to the specific elemental composition of the quaternary solid solution, which can be represented as a combination of the corresponding proportions of three binary compounds i. e. InAs, InSb and InP. It was shown that the change in the concentration of phosphorus and antimony during the solid solution deposition occurs synchronously. Moreover, the model of a gradient change in composition in epitaxial layers based on the system of In-As-Sb-P solid solutions when they are grown on the InAs substrate using the MOVPE [9] method was experimentally confirmed.

The active region in narrow-gap heterostructures obtained on InAs substrates can be represented by indium arsenide-antimonide compounds, where the $InAs_{1-y}Sb_y$ ternary solid solution is the result of the arsenic atoms replacement with antimony atoms in the crystal lattice of the indium arsenide. It is known that the additional element introduction into the solid phase leads to a deviation of the epitaxial layer composition of the ternary solid solution from the stoichiometric value, which is isomorphic to the substrate based on the binary compound. Consequently, with increase in the antimony concentration in the $InAs_{1-y}Sb_y$ layer, the mismatch relative to InAs increases, which, in turn, leads to increase in the internal stress in the heterostructure and, ultimately, to the destruction of the crystalline morphology of the layer. To compensate for internal stresses caused by mismatch between the lattice constants of compounds forming the epitaxial heterostructure, in practice a structural design of the „superlattice“ type is used based on various nanoscale layers from various systems of multicomponent solid solutions [4,10,11]. At the same time, this design also mades it possible to control the operating spectral range of the optoelectronic device. Previously, the narrow-gap InAsSb/InAsSbP quantum-size structure with phosphorus concentration in the solid phase of the barrier layer $x = 0.23$ demonstrated intense photoluminescence (PL) in the spectral range $3.18-3.75\,\mu$m [12].

As it was shown in [13,14], the type of the InAsSb/InAsSbP heterojunction can be transformed from the first to the second depending on the composition of the ternary solid solution. It was assumed that during the epitaxial growth using MOVPE method, the quality of the surface, on which deposition is performed, plays an important role and is a critical factor for the deposited compound. For example the $InAs_{1-y}Sb_y$ ternary solid solution to some extent affects the composition of the over growing InAsSbP quaternary solid solution. Then, with increase in the antimony concentration in the solid phase of the $InAs_{1-y}Sb_y$ layer ($y > 0.1$), vertical radiative transitions in a type I quantum well (superlattice) can transform into diagonal transitions in a type II quantum

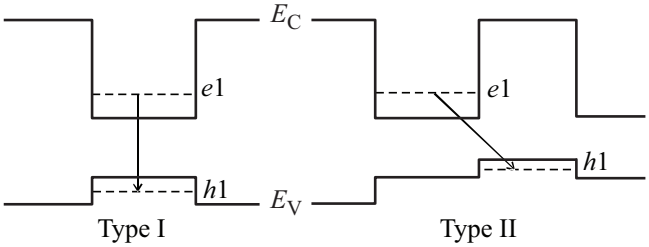


**Figure 1.** Schematic image of radiative transitions in quantum wells of type I and II. $e1$ and $h1$ — the ground levels of size quantization of electrons and holes, respectively. $E_C$ and $E_V$ — positions of bottom of the conduction band and the top of the valence band.

well (Figure 1). As can be seen from the Figure, the effective energy gap in the type II heterojunction is smaller than in the type I heterojunction. The use of type II heterojunctions makes it possible to move into the region of long wavelengths and to control Auger processes in the active region of an optoelectronic device [15,16]. This paper provides experimental evidence of change in the band energy structure of the quaternary solid solution layer during growth on surface of the epitaxial layer based on ternary compound of indium arsenide-antimonide.

## 2. Materials and samples for study

The heterostructures presented in this paper were obtained by the MOVPE method in a horizontal-type quartz reactor at atmospheric pressure on heavily-doped $n^+$-InAs:S (001) substrates with an excess electron concentration over $10^{18}\,\mathrm{cm}^{-3}$. The sources of components of the third and fifth groups for the epitaxial growth of the InAsSbP quaternary solid solution were the metalorganic compounds trimethylindium (TMIn), trimethylstibine (TMSb), tert-butylarsine (tBAs) and hydride gas phosphine ($PH_3$), diluted to concentration of 20% in hydrogen. The growth of the InAsSbP solid solution was carried out at temperature of 510°C. The composition of the injected vapor mixture during the each InAsSbP layer deposition was the same. The deposition time was 120 min, which ensured the deposited layer thickness about $h_B = 1000\,\mathrm{nm}$. The use of tBAs as a source of arsenic provided good predictability of the given composition when growing the $InAs_{1-x-y}Sb_yP_x$ solid solution with a high phosphorus content ($x > 0.4$) [8,9]. Sample $A$ is the heterostructure obtained by deposition of a single InAsSbP epitaxial layer directly onto the InAs substrate. Samples $B$ and $C$ were double heterostructures consisting of narrow-gap layer of the ternary $InAs_{0.95}Sb_{0.05}$ solid solution limited by two barrier layers based on the quaternary InAsSbP solid solution (Figure 2).

When depositing the InAsSb ternary solid solution the metalorganic compounds (TMIn and TMSb) and hydride gas arsine ($AsH_3$) were used as sources. Composition of the injected vapor mixture was the same during growing the $InAs_{0.95}Sb_{0.05}$ layer in the samples $B$ and $C$. The difference between these samples was during the deposition time: 3 min for sample $B$ and 180 min for sample $C$, which determined the thickness of each layer in $h_{QW} = 20\,\mathrm{nm}$ and $h_L = 1200\,\mathrm{nm}$ respectively.

Doping of the upper barrier layer with an acceptor impurity Zn for all structures under study ($n$-InAs/$p$-InAsSbP and $n$-InAs/$n$-InAsSbP/$n$-InAsSb/$p$-InAsSbP) was carried out in the same modes. Diethylzinc (DeZn) was injected into the reactor in 25 min before the end of the epitaxial structure growth. The amount of injected metalorganic compound for doping was the same.

The composition of the solid phase of the layers $InAs_{1-y}Sb_y$ and $InAs_{1-x-y}Sb_yP_x$ was determined using X-ray microanalysis data (CAMEBAX), studies of spectra of X-ray diffraction analysis (XDA) and secondary ion mass spectroscopy (SIMS). A layer of the quaternary $InAs_{1-x-y}Sb_yP_x$ solid solution deposited directly onto the InAs binary surface (sample $A$) was defined as $x = 0.41$ and $y = 0.19$. For sample $B$ the preliminary analysis of SIMS spectra indicated an increase in the concentration of antimony and phosphorus in the solid phase in absolute value in the top barrier layer of InAsSbP compared to the bottom barrier layer (Figure 2, *a*). The results of studying the XDA spectra for the sample $C$ are presented in the paper [17]. Since the top layer of InAsSbP in samples $B$ and $C$ was deposited on the surface of the ternary InAsSb solid solution, the composition of these layers could differ from what was originally planned. As mentioned above, the antimonide presence in the crystalline structure of the InAsSb epitaxial layer, along with change in the surface lattice constant, led to increase in antimony and decrease in phosphorus in the solid phase of the grown barrier layer [13].

To measure the PL spectra a Bruker Vertex 80v vacuum Fourier spectrometer was used in step-by-step scanning mode together with an external chamber for experiments with an additional modulated beam. It was equipped with a liquid nitrogen-cooled InSb photodetector, a KBr beam splitter and a semiconductor laser diode with wavelength of 532 nm and power of 130 mW, which provided optical pumping. Phase-sensitive detection of the optical response was performed using a lock-in amplifier. A similar approach based on the Fourier transform of the recorded signal was demonstrated as an effective tool for the optical characterization of the materials with narrow band gap in the mid-infrared spectral range [18–20].

## 3. Experimental results and discussion

The PL spectra at room temperature ($T = 300\,\mathrm{K}$) for the heterostructures under study contained emission bands in the photon energy region 0.25−0.65 eV (Figure 3). The sample $A$ demonstrated one clearly defined emission band $h\nu_H^{300}$, the maximum intensity of which was near 0.5 eV. In turn, for samples $B$ and $C$ in the photon energy region 0.25−0.4 eV another emission band was observed in

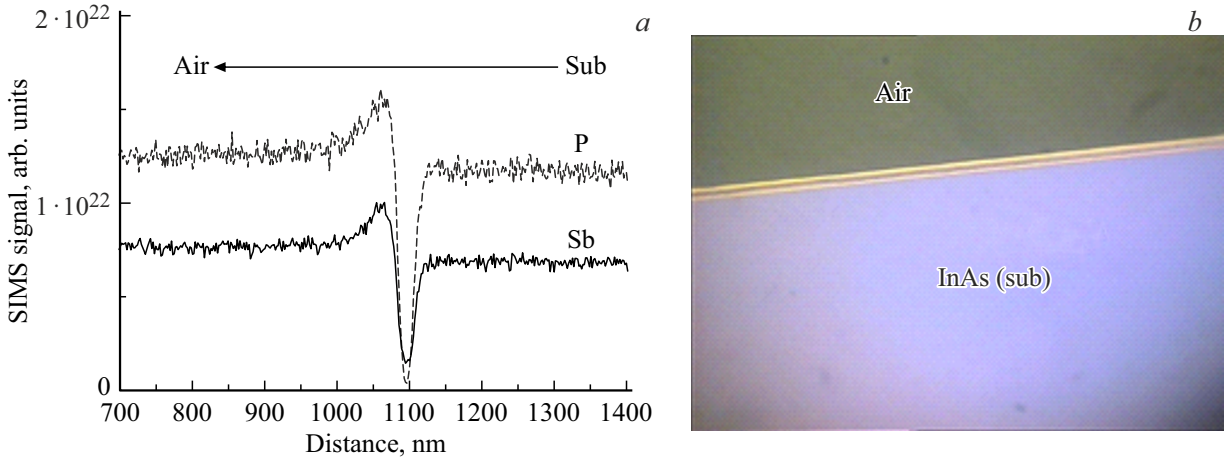


**Figure 2.** *a* — SIMS spectra for phosphorus (dashed line) and antimony (solid line) for the sample *B* (structure InAsSbP/InAsSb/InAsSbP). The distance is measured from the outer surface of the heterostructure. *b* — image of the cross-section of the sample *C*. Light stripes — InAsSbP layers, dark stripe between them — $InAs_{0.95}Sb_{0.05}$ layer. InAs substrate has the same contrast as the later of the narrow-gap ternary solid solution.

addition to the high-energy band mentioned above. The maximum intensity of the high-energy PL band for the sample *C* was quite easily determined near the value of 0.449 eV, while for the sample *B* the band $h\nu_H^{300}$ looked like the shoulder of a more intense low energy band. Analyzing the PL spectrum for the sample *B* as a result of the superposition of two peaks with Gaussian intensity distribution, the maximum of the band $h\nu_H^{300}$ was determined near photon energy values 0.468 eV, which exceeded the value found for the sample *C*. We attribute the observed high-energy PL bands for all studied heterostructures to emission recombination transitions in the bulk of the wide-gap $InAs_{1-x-y}Sb_yP_x$ quaternary solid solution and associate them with emission from the top barrier layer, since there is a high probability of absorption the luminescence from the bottom barrier layer by the above layer of narrow-gap ternary solid solution. Different values of the spectral position of the maximum of the high-energy band in the PL spectra at $T = 300$ K (Figure 3) indicate the obvious dependence of the band gap of the deposited InAsSbP solid solution on the type of matrix surface on which deposition was carried out. A similar PL behavior was observed previously for double InAsSbP/InAsSb/InAsSbP heterostructures with quantum wells based on narrow-gap layers of the $InAs_{0.87}Sb_{0.13}$ ternary solid solution of various thicknesses [21].

To calculate the band gap of the $InAs_{1-x-y}Sb_yP_x$ quaternary solid solution we used the following general expression:

$$E_{G,\mathrm{InAs}_{1-x-y}\mathrm{Sb}_y\mathrm{P}_x} = E_{G,\mathrm{InAs}} \cdot (1-x-y) + E_{G,\mathrm{InSb}} \cdot y + E_{G,\mathrm{InP}} \cdot x - C_{\mathrm{InAsP}} \cdot (1-x-y) \cdot x - C_{\mathrm{InAsP}} \cdot (1-x-y) \cdot y - C_{\mathrm{InSbP}} \cdot x \cdot y, \quad (1)$$

where $E_{G,ij}$ — band gap of binary compound forming a quaternary solid solution [22], $C_{ijk}$ — coefficients considering non-linear dependence of parameter $E_G$ on composition considering formation of ternary compounds [13]. Assuming that the photon energy of the PL band at $T = 300$ K can be comparable with the band gap of the quaternary solid solution, we calculated the compositions of the capping epitaxial layers for each heterostructure.

From the PL spectra presented in Figure 3, it can be determined that the spectral position of the maximum of the low-energy band $h\nu_L^{300}$ for the sample *B* (0.343 eV) locates by 25 meV higher than for the sample *C* (0.318 eV). Besides, the emission bandwidth at half maximum was 38 and 48 meV, respectively. Taking into account the band gap of the $InAs_{0.95}Sb_{0.05}$ solid solution according to formula (1) equal to 0.316 meV, the experimentally observed increase in the emission transition photon energy and narrowing of the luminescence band for the sample *B* indicate a sufficient degree of localization of charge carriers involved

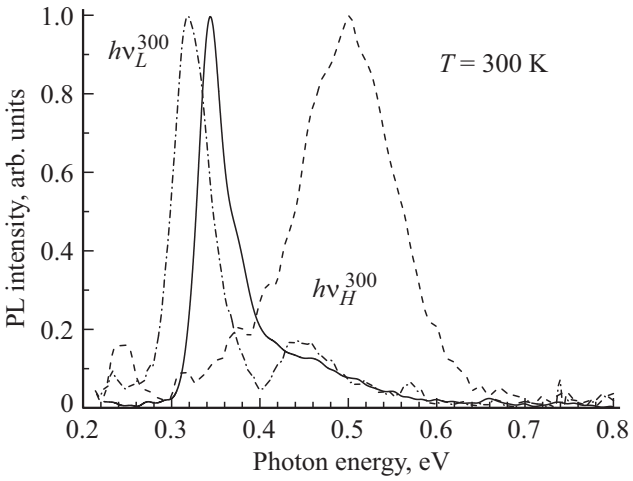


**Figure 3.** PL spectra at room temperature for sample *A* (dashed line), sample *B* (solid line) and sample *C* (dashed-dotted line).

**Table 1.** Calculated values for band gaps of the $InAs_{1-x-y}Sb_yP_x$ quaternary solid solution in samples under study at various temperatures

| Sample | P in solid phase ($x$) | Sb in solid phase ($y$) | $E_G(300)$ ($T = 300$ K) | $E_G(80)$ ($T = 80$ K) | $E_G(4)$ ($T = 4$ K) |
|---|---|---|---|---|---|
| *A* | 0.406 | 0.19 | 0.501 eV | 0.561 eV | 0.57 eV |
| *B* | 0.39 | 0.21 | 0.468 eV | 0.529 eV | 0.538 eV |
| *C* | 0.375 | 0.22 | 0.448 eV | 0.509 eV | 0.518 eV |

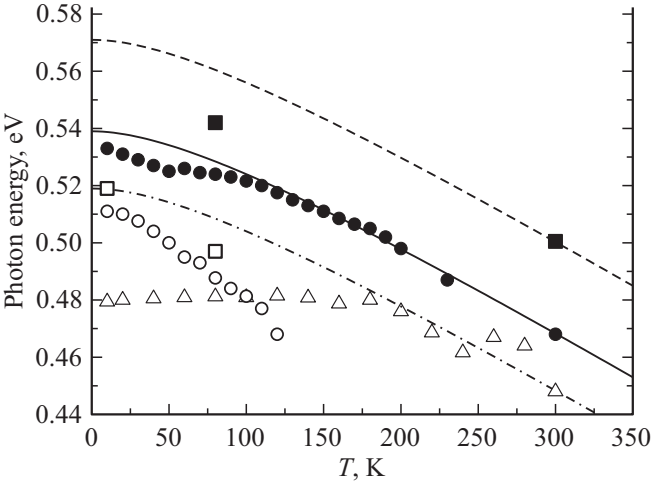


**Figure 4.** Temperature dependences of photoluminescence and calculated data: sample *A* — dashed line and squares (experimental data from paper [17]), sample *B* — solid line and circles (experimental results from this paper), sample *C* — dash-dotted line and triangles (experimental data from this paper [17]).

in recombination, which can be realized in quantum-sized structures. Using the platform capabilities [23], we have calculated the band energy diagram of a 20 nm-wide single quantum well (QW) with the type I alignment ($InAsSbP/InAs_{0.95}Sb_{0.05}/InAsSbP$), and determined the positions of the main size quantization levels for electrons and holes $e_1 = 0.022$ eV and $h_1 = 0.001$ eV, respectively. It is obvious that increase in the width of the narrow-gap layer leads to decrease in the energy of localization levels. Taking into account the energy values of size quantization levels in the resulting QW, it is possible to explain the different positions of low-energy PL bands for samples *B* and *C*.

In a similar way, using formula (1), we have also obtained the calculated values of the band gap at $T = 4$ K and $T = 80$ K for each quaternary solid solution presented in Table 1. This table shows that presence of layer of the $InAs_{0.95}Sb_{0.05}$ ternary solid solution of different thickness leads to change in the solid phase composition of the over grown quaternary solid solution. Based on the data obtained, the temperature dependences of the band gap were plotted for each sample, the dependences passed through the calculated values corresponding to photon energies for temperatures 4, 80 and 300 K (Figure 4). As a result, for all the heterostructures under study the Varshni dependence was applied in general form:

$$E_G = E_i - 3.3 \cdot 10^{-4} \frac{T^2}{(T + 120)}, \qquad (2)$$

where $E_i$ — band gap at $T = 0$ K, typical for each sample (*A* — 0.571 eV, *B* — 0.54 eV and *C* — 0.519 eV). As Figure 4 shows, a good agreement between the calculated curve and experimental data for sample *B* and *C* was achieved at high temperatures ($T > 150$ K). Energy of experimental PL data at low temperatures was below the energy of calculated curves for all heterostructures under study. At the same time, samples *A* and *B* demonstrated two groups of temperature dependences for PL in the low-temperature range, while sample *C* was characterized by one emission band over the entire temperature range.

The full PL spectrum for the sample *B* over the entire temperature range contained two pronounced emission bands: low-energy band near $h\nu_L^B = 0.37$ eV and high-energy band in the range 0.44–0.54 eV. As already mentioned, the high-energy band at low temperatures ($T < 80$ K) was a doublet structure, in which two components can be distinguished: $h\nu_1^B$ and $h\nu_2^B$ (Figure 5). Intensity of band $h\nu_2^B$ prevails at low temperatures, while upon temperature increasing ($T > 80$ K) the band $h\nu_1^B$ becomes dominant. Thus, different rates of temperature quenching of PL were observed in the high-energy part of the spectrum. Note that different nature was revealed in spectral shift for these components towards lower photon energies relative to the design curve of the barrier layer band gap with increasing temperature.

The temperature shift for the band $h\nu_1^B$ at high temperatures ($T > 150$ K) is well described by the calculated curve (Figure 4, closed circles), obtained according to expression (2) and displaying the temperature dependence of the band gap of the $InAs_{0.4}Sb_{0.21}P_{0.39}$ quaternary solid solution. Since at temperatures near room temperature the band $h\nu_1^B$ corresponds to interband radiative transitions (edge luminescence), then with decrease in temperature ($T < 80$ K) a restructuring of recombination processes and a transition to emission processes involving shallow localized states inside the band gap of the top barrier layer can occur. The energy of such states occurrence was about 6 meV at helium temperatures. It is not difficult to calculate that when the temperature rises above 100 K ($k_BT \sim 8.5$ meV) the charge carriers can leave these states under the influence of thermal energy and move to the region of energy bands.

Band $h\nu_2^B$ shows the opposite trend in temperature dependence (Figure 4, open circles). First, this PL band can be attributed to radiative recombination transitions involving deep states inside the band gap with energy of occurrence over 28 meV ($T = 4$ K). Second, the band $h\nu_2^B$ shows a strong red shift (shift towards low photon energies) with temperature increasing. A similar temperature dependence of the spectral position of PL band maximum was observed previously for undoped In(As, Sb)P epitaxial layers with high InP content in the solid phase, grown by molecular beam epitaxy [24]. Since this paper considers layers of the quaternary solid solution containing $x > 0.4$, then deep donor states in the band gap can be initiated by natural structural defects caused by the indium phosphide presence. The steep slope of redshift of band $h\nu_2^B$ is most likely due to thermal tunneling between charge carrier localization regions formed as a result of overlapping density tails of donor states. This tunneling process allows charge carriers to move into lower energy states as the temperature increases. Besides, at low temperatures the quenching of $h\nu_2^B$ band with temperature increasing occurred faster than for $h\nu_1^B$ band (Figure 5), and at $T > 150$ K it almost did not appear in the PL spectra. Since edge luminescence was simultaneously observed, this means that the majority of charge carriers trapped in deep states left the localization site under the influence of thermal energy in a non-radiative manner.

It is known that in addition to radiative transitions in the recombination of charge carriers, there are also non-emission processes that significantly affect the luminescent properties of narrow-gap compounds. To determine the nature of non-radiative recombination processes in the InAsSbP quaternary solid solution, the temperature dependence of the integrated intensity of the high-energy band for the sample $B$ was studied (Figure 6). The PL intensity curve showed a smooth exponential decrease with temperature increasing, and in absolute value the intensity decreased by 4 times only in the range between 50 and

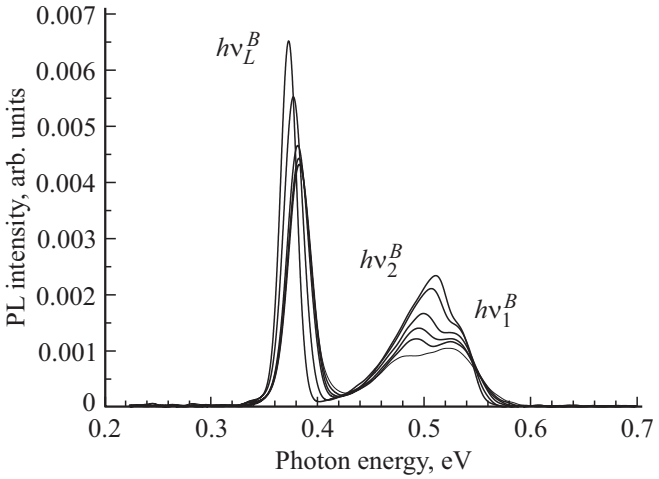


**Figure 5.** PL spectra for the sample $B$ for the temperature range from 10 to 90 K.

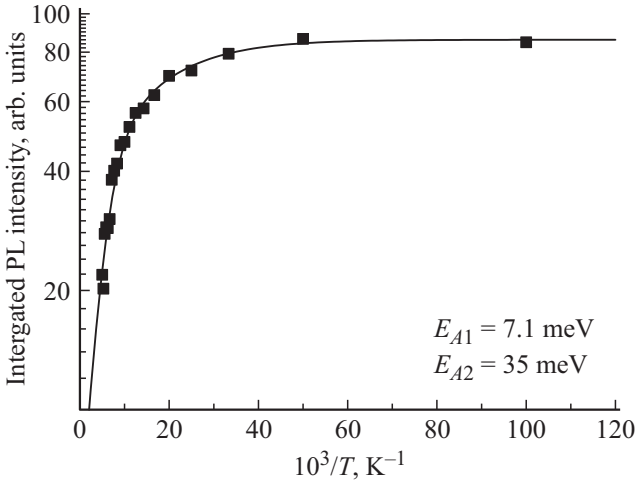


**Figure 6.** Temperature dependence of the integral intensity of high-energy band in the PL spectrum for sample $B$.

200 K. The resulting dependence, as a rule, is described by the Arrhenius formula [25], indicating thermally activated mechanisms of non-radiative recombination, to determine the thermal activation energy of states formed by defects. This temperature dependence can be expressed by the following formula:

$$I_{\text{int}} = \frac{I_0}{(1 + B_1 e^{(-E_{A1}/k_B T)} + B_2 e^{(-E_{A2}/k_B T)}}, \qquad (4)$$

where $B_i$ — the ratio of the probabilities of non-radiative recombination to radiative one for $i$-th thermally active process of the non-radiative recombination mechanism at 300 K, $E_{Ai}$ — its corresponding thermal activation energy, $k_B$ — Boltzmann's constant. Since the approximation of the experimental curve points obtained from the first-order Arrhenius equation, in which only one non-radiative channel was assumed, did not give good agreement with experiment, we assumed that the dissociation process involves two non-radiative activation channels, as was proposed for the case of bound excitons in GaAs [26]. Then customization based on the second order equation (4) with rate constants $B_1$ and $B_2$, and activation energies $E_{A1}$ and $E_{A2}$ [27], gives good agreement with experimental data when using the parameters $B_1 = 15$, $B_2 = 1.3$, $E_{A1} = 7.1$ meV and $E_{A2} = 35$ meV, respectively. It can be seen that at high temperatures the first channel dominates in non-radiative recombination (with a higher activation energy $E_{A1}$), and at a relatively low temperature the second non-radiative channel dominates in the process of non-radiative recombination (with a lower activation energy $E_{A2}$). The activation energy $E_{A1} = 7$ meV for temperatures below 100 K suggests that it is associated with the ionization of impurity-bound excitons and is the sum of the localization energy and the exciton bond energy [28]. This small activation energy may also be associated with the fluctuations of the barrier layer potential.

The increase in temperature allows charge carriers to gain sufficient kinetic energy to be released from the

localized state and move to the vicinity of a non-radiative recombination center. It is possible, that deep traps due to the presence of a deep donor, a neutral impurity, or a vacancy-related defect are also the most likely cause of the activation energy $E_{A2} = 37$ meV. The probability of non-radiative transition may increase due to change in the nature of the crystalline structure ordering. At low temperatures PL efficiency is controlled by carrier thermalization due to localized fluctuations of the energy band edge, whereas at higher temperatures in photoluminescence the non-radiative transitions prevail, they are most likely to occur in the most disordered solid solution. Although this simple model adequately describes the temperature behavior of PL, the exact nature of the thermally activated loss mechanisms remains a matter of assumptions.

Some feature in the formation of the crystalline structure of the epitaxial layer in the system of In-As-Sb-P quaternary solid solutions is noted. As can be seen from the abbreviation of this $A^3B^5$ compound, it can be represented as a combination of three binary compounds InAs-InSb-InP in the appropriate proportion, since the component of III group (In) is common to the remaining atoms, representatives of V group. As was shown earlier [8], the quasi-ternary compound In(As, Sb, P) has the effect of self-organization of the solid phase during epitaxial deposition, i. e. the total concentration of components of V group in the solid solution remains unchanged. Then, if the conditions of isomorphism of the grown heterostructure are met, the increase in the antimonide concentration in the solid phase of the $InAs_{1-y}Sb_y$ layer on which deposition is carried out, leads to increase in the antimonide concentration in the over grown top barrier layer and, consequently, to decrease in the percentage of phosphide. In this case, the fraction of arsenide as the basic component of the epitaxial heterostructure grown on the InAs substrate is retained (Table 1). As a result, the fraction of the wide-gap component of the quaternary solid solution (InP) will decrease, while the fraction of the narrow-gap component (InSb) will increase. Since the band gap of InAs is closer to the band gap of InSb compared to InP, the ratio between the wide-gap and narrow-gap components of the quaternary solid solution can be written as P/(As + Sb). As can be seen from Table 2, with the ratio P/(As + Sb) decreasing the energies of occurrence of recombination centers decrease.

According to Table 1, from all presented barrier layers the sample *A* demonstrates the maximum phosphorous concentration in solid phase for the $InAs_{0.404}Sb_{0.19}P_{0.406}$ epitaxial layer. It was established that among the heterostructures under study the energy distance between the calculated value of the band gap and the experimental values of the photon energy at the maximum of the PL emission bands was also found to be greatest for the sample *A*. Thus, the predominance of the narrow-gap component of the solid phase in the quaternary solid solution over the wide-gap component is expressed in decrease in the effective occurrence energy for charge carrier localization centers in the band gap of the epitaxial layer. As a result, a situation arises when the doublet structure of the high-energy PL band is transformed into a single emission band (Figure 7).

**Table 2.** The difference in photon energies between the calculated value of the band gap of the quaternary solid solution ($E_G$) and the spectral position of the maximum intensity of the PL band from the top InAsSbP layer ($h\nu_i^B$) in the samples under study

| Sample | P/(As + Sb) solid phase | $T = 4$ K $E_G - h\nu_2^B$, meV | $T = 80$ K $E_G - h\nu_2^B$, meV | $T = 80$ K $E_G - h\nu_1^B$, meV |
|---|---|---|---|---|
| *A* | 0.683 | 53 | 65 | 19 |
| *B* | 0.639 | 28 | 39 | 6 |
| *C* | 0.6 | 38 | 28 | – |

Note that values for activation energies in formula (4) of the sample *B* are in good agreement with values of occurrence energies for components of the high-energy PL band.

Consider that epitaxial growth of the $InAs_{1-x-y}Sb_yP_x$ layers is performed at same initial technological conditions, but deposition was performed on different matrix surfaces. In the case of the sample *A*, the epitaxial deposition was performed directly on the surface of binary compound (InAs substrate) and the quaternary solid solution layer was isomorphic to the substrate. In samples *B* and *C*, the top barrier layer of InAsSbP was grown on the surface of the $InAs_{0.95}Sb_{0.05}$ ternary solid solution. Due to the features of thermodynamic processes during deposition by the MOVPE method, the grown solid solution is the result of chemical reactions of metalorganic compounds over the matrix surface on which deposition occurs [8,9]. Accordingly, the epitaxial layer will be isomorphic to the compound on which it is being grown. For the sample *C* it was experimentally established that the mismatch between

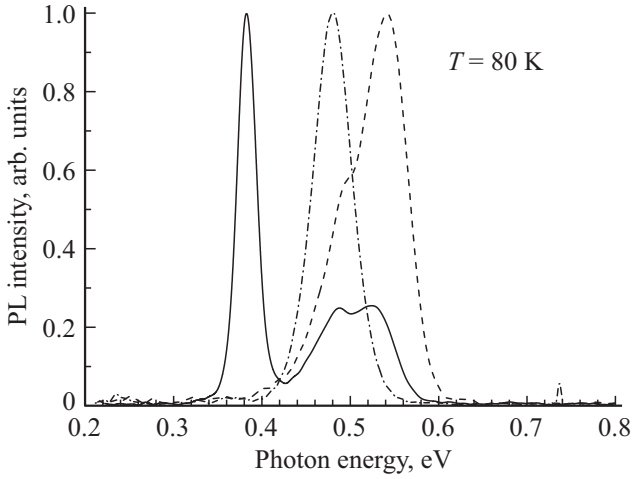


**Figure 7.** PL spectra at liquid nitrogen temperature (sample *A* — dashed line, sample *B* — solid line, sample *C* — dashed-dotted line).

the $InAs_{0.95}Sb_{0.05}$ ternary solid solution layer and the $InAs_{1-x-y}Sb_yP_x$ barrier layer grown on it reached about $3.5 \cdot 10^{-3}$ with respect to the InAs substrate [17]. In this case, the mismatch calculated using expression (3) for the $InAs_{0.405}Sb_{0.22}P_{0.375}$ layer, the composition of the solid phase of which was determined from measurements of PL spectra at $T = 300$ K, and showed good agreement with experimental data obtained from XDA measurements.

The estimate of the lattice constant of multicomponent solid solution can be made using the example of a linear approximation proposed in paper [29]:

$$a_{InAs_{1-x-y}Sb_yP_x} = a_{InAs} \cdot (1 - x - y) + a_{InSb} \cdot y + a_{InP} \cdot x, \quad (3)$$

where $a_i$ — crystal lattice constant parameter of binary compounds forming the $InAs_{1-x-y}Sb_yP_x$ quaternary (quasi-ternary) solid solution. Using the data from Table 1, we can evaluate the mismatch of the top barrier layer relative to the InAs substrate for samples *A* and *B*, which was about $0.5 \cdot 10^{-3}$ and $2.1 \cdot 10^{-3}$ respectively. A similar change in the lattice constant of the quaternary solid solution was previously observed for a single quantum well InAsSbP/$InAs_{0.87}Sb_{0.13}$/InAsSbP [21]. Thus, the layer of the top barrier InAsSbP with a preliminary mismatch relative to the substrate about $-5 \cdot 10^{-3}$ demonstrated mismatch equal to $-1.2 \cdot 10^{-3}$ when oven grown on the quantum-sized layer ofthe $InAs_{0.87}Sb_{0.13}$ ternary solid solution as thick as 5−20 nm.

The difference between the samples *B* and *C* was that in the sample *B* the active region of the heterostructure was a layer 20 nm thick, then as in the sample *C* the narrow-gap layer had thickness of 1200 nm. Consequently, in sample B the InAsSb layer can be stressed (elastic compression) due to the specific formation of quantum-size structure when it is located between thick barrier layers with similar crystal lattice constants. Then, the mismatch of the quantum-size layer relative to the InAs substrate is partially compensated due to the internal stress of the heterostructure, and under all other technological conditions of the epitaxial process, the layer of the InAsSbP quaternary solid solution is grown onto layer that has an effective lattice constant less than in the case of a relaxed thick layer (sample *C*). Accordingly, the band gap of the top barrier layer of InAsSbP, determined by the composition of the solid solution, will be smaller than in the sample *A*, but larger than in the sample *C* (Table 1).

## 4. Conclusion

Thus, the elemental composition of the matrix surface and the presence of internal stress between the layers of the epitaxial heterostructure affect the composition of multicomponent solid solutions obtained by the MOVPE method on the surface of indium arsenide-antimonide compounds. The change in the composition of InAsSbP covering layers determines the type of energy band diagram of In(As, Sb)/InAsSbP heterostructure. Besides, there is a tendency in change of the band gap and the occurrence energy for localized states in the band gap of the solid solution depending on the degree of internal disorder of the top barrier layer when deviating from isomorphic composition relative to InAs substrate. The predominance of the narrow-gap component of the solid phase in the quaternary solid solution over the wide-gap component is expressed in decrease in the effective occurrence energy for charge carrier localization centers in the band gap of the epitaxial layer.

### Acknowledgments

The authors express their sincere gratitude to M. Motyka and T. Smołka for their assistance in carrying out photoluminescence studies and useful discussions of the results obtained, and Yu. Kudryavtsev for assistance in carrying out SIMS measurements.

### Conflict of interest

The authors declare that they have no conflict of interest.

## References

[1] I.A. Andreev, M.A. Afrailov, A.N. Baranov, M.P. Mikhailova, K.D. Moiseev, V.V. Sherstnev, V.E. Umansky, Yu.P. Yakovlev. Pis'ma v ZhTF **16**, *4*, 27 (1990). (in Russian).
[2] A.N. Baranov, A.N. Imenkov, V.V. Sherstnev, Yu.P. Yakovlev. Appl. Phys. Lett. **64**, 2480 (1993).
[3] B. Lane, M. Razeghi. J. Cryst. Growth **221**, 679 (2000).
[4] A. Behres, D. Puttjer, K. Heime. J. Cryst. Growth **195**, 373 (1998).
[5] J. Devenson, R. Teissier, O. Cathabard, A.N. Baranov. Appl. Phys. Lett. **90**, 111118 (2007).
[6] K.D. Moiseev, Yu.P. Yakovlev. Interface lasers with asymmetric band offset confinements. Chapter in book: Mid-Infrared Semiconductor Optoelectronics / Ed. A. Krier. Springer. Ser. in Opt. Sci. (2006). P. 219–235.
[7] R.M. Biefeld, K.C. Baucom, S.R. Kurtz, D.M. Follstaedt. J. Cryst. Growth **133**, 38 (1993).
[8] V.V. Romanov, M.V. Baidakova, K.D. Moiseev. Semicond. **48**, *6*, 733 (2014).
[9] K.D. Moiseev, V.V. Romanov, Yu.A. Kudryavtsev. Phys. Solid State **58**, *11*, 2285 (2016).
[10] B. Lane, Z. Wu, A. Stein, J. Diaz, M. Razeghi. Appl. Phys. Lett. **74**, 3438 (1999).
[11] T. Fukui, Y. Horikoshi. J. Jpn. Appl. Phys. **19**, L551 (1980).
[12] C.J. Wu, G. Tsai, H.H. Lin. Appl. Phys. Lett. **94**, 211906 (2009).
[13] K.D. Moiseev, V.V. Romanov. Phys. Solid State **63**, *4*, 566 (2021). doi: 10.21883/FTT.2021.04.50712.260
[14] A.A. Semakova, M.S. Ruzhevich, V.V. Romanov, N.L. Bazhenov, K.D. Mynbaev, K.D. Moiseev. Semicond. **56**, *9*, 659 (2022). doi: 10.21883/SC.2022.09.54131.9925
[15] A.A. Semakova, V.V. Romanov, N.L. Bazhenov, K.D. Mynbaev, K.D. Moiseev. Semicond. **55**, *3*, 354 (2021). doi: 10.21883/FTP.2021.03.50607.9549.
[16] V.V. Romanov, E.V. Ivanov, K.D. Moiseev, A.A. Pivovarova, Yu.P. Yakovlev, Semicond. **54**, *2*, 253 (2020).

[17] T. Smołka, M. Motyka, V.V. Romanov, K.D. Moiseev. Materials **15**, 1419 (2022).
[18] D.D. Firsov, O.S. Komkov. Pis'ma v ZhTF **39**, *23*, 87 (2013). (in Russian).
[19] T.J.C. Hosea, M. Merrick, B.N. Murdin. Phys. Status Solidi **202**, *7*, 123 (2005).
[20] J. Shao, W. Lu, F. Yue, X. Lü, W. Huang, Z. Li, S. Guo. Rev. Sci. Instrum. **78**, *1*, 13111 (2007).
[21] M. Kurka, M. Dyksik, W. Golletz, M. Środa, V.V. Romanov, K.D. Moiseev, M. Motyka. Appl. Phys. Exp. **12**, 115504 (2019).
[22] Landolt-Börnstein. Handbook. Numerical Data. Ser. III. / Ed. O. Madelung. Springer, Berlin, Heidelberg (1982). 17a. 264 p. / Ed. K.-H. Hellwege (1987). 22a. 305 p.
[23] http://www.matprop.ru/levels/index.php
[24] G. Tsai, D.L. Wang, H.H. Lin. J. Appl. Phys. **104**, 023535 (2008).
[25] F.D. Auret, N.A. Bojarczuk, C.P. Schneider. J. Vac. Sci. Tech. B **3**, 853 (1985).
[26] D. Bimberg, M. Sondergeld, E. Grobe. Phys. Rev. B **4**, 3451 (1971).
[27] M. Leroux, N. Grandjean, B. Beaumont, G. Nataf, F. Semond, J. Massies, P. Gibart. J. Appl. Phys. **86**, 3721 (1999).
[28] F. Luckert, M.V. Yakushev, C. Faugeras, A.V. Karotki, A.V. Mudryi, R.W. Martin. J. Appl. Phys. **111**, 093507 (2012).
[29] L. Vegard. Z. Phys. **5**, 17 (1921).

*Translated by I.Mazurov*